Wear 394–395 (2018) 159–165

Contents lists available at ScienceDirect

Wear

journal homepage: www.elsevier.com/locate/wear

Case study: The effect of running distance on the microstructure and properties of railroad axle bearings

Rubing Guo[a], Xianqi Lei[b], Dongdong Zhang[c], Zhiming Liu[a], Xi Wang[a], Yujie Wei[a,b,*]

[a] Engineering Research Center of structure Reliability and Operation Measurement Technology of Rail Guided Vehicles of MOE, Beijing Jiaotong University, Beijing 100044, China

[b] LNM, Institute of Mechanics, Chinese Academy of Sciences, Beijing 100190, China

[c] Beijing Railway Bureau, Beijing 100860, China

ARTICLE INFO

Keywords:
Bearing steel
Fracture toughness
Gradient structure
Grain refinement

ABSTRACT

As a key component, axle bearings play an important role in transmission systems. Motivated by the rapid growth of railway network and the significance of bearing safety, we report here how different operating duration may alter the macroscopic and microscopic mechanical property of high speed train axle bearing's outer ring made of GCr15 steel, a high-carbon chromium bearing steel known for its superb contact fatigue resistance, good dimensional stability and excellent corrosion resistance. We characterized the structural and mechanical properties of the load carrying zone at operating duration of new, 1.2 Mkm and 2.4 Mkm bearing. In contact to the as-received ones, the outer ring samples show clear grain refinement, exhibit inhomogeneous hardness distribution and show a decrease of about 42% for the tensile elongation after 2.4 Mkm operation.

1. Introduction

Bearings are ubiquitous in industrial machinery. They are widely used to transmit rotary motion and support radial and thrust loads. As a result, their reliability is crucial for the safety of associated mechanical systems. With engineers are pushing the limit of machines for high power, high speed and large load capacity, there is growing interest in designing and manufacturing high quality bearings for those advanced applications. That is particularly true in the high speed railways (HSR) industry where axle-bearings of extremely high performance are desired for increasing demand of faster speed. More importantly, axle-bearing failure is such a serious issue often resulting in operation delays and even potentially derailment that they receive extra attention during regular maintenance.

Commonly used axle-bearings in HSR are composed by outer ring, inner ring, roller, bearing cage and grease. The bearing outer ring is fixed and rolled by the bearing rollers during bearing operating condition which is shown in Fig. 1. The bearing maintenance duration in China is 1.2 Mkm (1.2 Mkm~4×10^8 cycles). Such bearings are made of ultra-high strength steel with a tensile strength exceeding 2.7 GPa and hardness values beyond 900 HV [1]. During the maintenance, it is found that typical failure modes in bearings include peeling and fatigue of the bearing outer ring, which occur in the loading area shown in Fig. 1. Fatigue in bearings is of the rolling contact fatigue, which can result from both surface and sub-surface initiated microcracks. For the former, surface cracks often originate from contaminated lubricants; foreign particles entrained in the moving elements of the bearing produce wear or denting of the bearing surfaces. As to the later, microcracks embryo from the interface of matrix and second-phase hard particles, and grow gradually under cyclic loading.

The bearing damage [2–7] spotlighted the subsurface plastic residual strains after the application of shear-stress loops [4]. Models [2,6] were developed to predict the fatigue damages appearing at the subsurface. Lei [7] noticed that very high cycle fatigue crack tends to start from interior grain boundary with fine granular area at the initiation in GCr15 bearing steel. These wear particles usually initiated from the local plastic deformation of the operating surfaces [8–11]. Lu et al. [12] showed that surface mechanical attrition treatment [13], a technique similar to the scenarios of bearings in contact, may lead to a gradient hierarchical structure. Such gradient structure is believed to achieve better mechanical strength while retaining the ductility of coarse-grained counterpart [14,15]. In particular, it could enhance the materials anti-fatigue performance [16]. For examples, the hardness increases gradually from about 1.85 GPa in the matrix to about 3 GPa in the nanocrystallized subsurface [17]. The subsurface hardness increases with depth in the bearing steel [18]. Many groups demonstrated that

* Corresponding author at: Engineering Research Center of structure Reliability and Operation Measurement Technology of Rail Guided Vehicles of MOE, Beijing Jiaotong University, Beijing 100044, China.
E-mail address: yujie_wei@lnm.imech.ac.cn (Y. Wei).

http://dx.doi.org/10.1016/j.wear.2017.10.016
Received 21 August 2017; Received in revised form 17 October 2017; Accepted 30 October 2017
Available online 31 October 2017

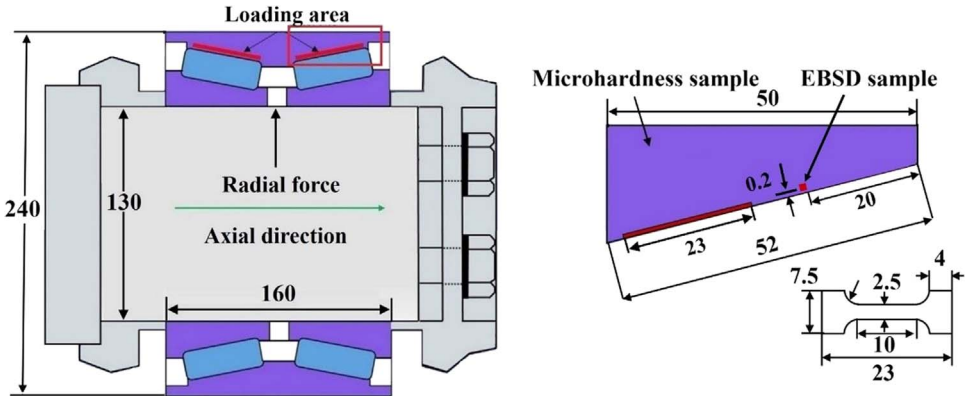

Fig. 1. The assemble illustration of the HSR bearing, and the region marked by the red lines are the loading contact zones between conical rollers and outer ring. The hardness samples are sliced from the red box area. Samples for EBSD test are chosen from the loading area. The uniaxial tensile samples are machined from the near rolling surface as marked by the red line in the right figure, and the exact dimensions are at the bottom right corner. All samples have a thickness of 0.5 mm. The axle load of the train is 17 t and the weight of wheel is 1.5 t, which corresponds to an applied load of about 3.7 kN and further to a maximum Hertz contact stress of about 1.23 GPa in the loading area of the outer ring.

the microstructural evolution affects the wear performance and rolling contact fatigue property in the subsurface of bearing steel [19–22]. So far, there are no clear conclusions about the damage evolution for these bearings. The focus of this paper is to examine the microstructure evolution of the bearing outer ring and build a connection between the evolution of microstructures with the macro and micro-scopic mechanical property of the bearing outer ring.

2. Material and experiments

The bearing outer ring is made of a high carbon chromium steel, named 100Cr6 in Europe and GCr15 in China, which element composition is analyzed by inductively coupled plasma mass spectrometry (ICP-MS) method and listed as in Table 1.

The raceway surface profiles after different operating durations are characterized by using CV-3100 Stylus Profiler. The results are shown in Fig. 2. It can be seen that the raceway surfaces, from the initial convex profiles, are worn into concave ones. The wearing rate is on the order of 7 μm/Mkm. Such significant wearing amount would then subsequently influence the dynamic performance of the bearings.

2.1. Microstructure characterization

X-ray diffraction (XRD) and scanning electron microscopy (SEM) combined with electron backscatter diffraction (EBSD) systems are exploited to evaluate the outer ring's microstructure evolutions, and the samples are cut from the contact zone of the outer rings. For the XRD characterization, the samples are grinded mechanically to an end of 5000 grade sandpaper, and the phase composition of the samples at room temperature is determined with an X-ray diffractometer (Rigaku MiniFlex II). For the SEM micrograph observation, the samples are first mechanically polished, then etched using a 2 vol% nitric acid ethanol solution at room temperature. For the EBSD characterization, the mechanically polished surfaces of the samples are further polished in colloidal silica suspension for 2 h to yield a stress-free surface for high quality EBSD images. The SEM and EBSD characterization are performed on a JEOL 6500 F test platform.

2.2. Uniaxial tensile test

The specimens are cut near the loading area of the outer ring by electro discharge machining (EDM) method, and the sample dimensions are shown in Fig. 1. The samples are first mechanically grinded to an end of 5000 grade water sandpaper, and then electrolytic polished in a 5 vol% glacial acetic acid ethanol solution (at temperature of 291 K and voltage of 37 V) to achieve a mirror-polished finished surface and remove the surface residual stress at the same time. A SANS test system is employed to conduct the test. The gauge length of the sample is 5 mm. The strain rate is set to 10^{-3} s^{-1}. For bearings of different operating duration, we conducted 5 independent tests to ensure the repeatability of results.

Table 1
Chemical composition of material (mass %).

C	Cr	Mn	Ni	Si	Mo	W
0.98	1.35	0.39	0.16	0.30	0.05	< 0.005

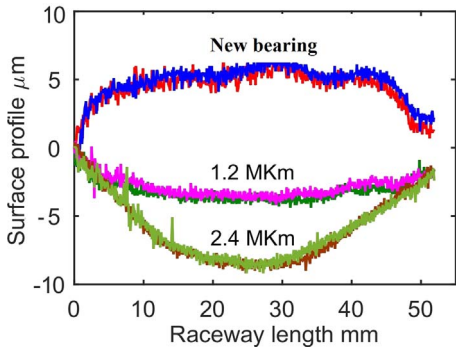

Fig. 2. The raceway surface profiles for new, 1.2 Mkm and 2.4 Mkm operating bearings. Significant wearing in bearings is seen. Even the profile varies dramatically. Two independent tests had been carried out for each type of bearings.

2.3. Microhardness test

The samples for hardness measurements are sliced from the cross-section of the bearing outer ring (boxed zone in Fig. 1), mechanically grinded to an end of 5000 grade water sandpaper, and then polished to a mirror finished surface. The Vickers hardness of the sample is measured by a micro-hardness tester MH-6. A diamond Vickers indenter with a face angle of 136° is used. The hardness is measured under a load of 300 g and a holding time of 10 s at room temperature. The measurements are conducted row by row, with row spacing of 0.1 mm along the normal direction of the contact surface for the first 10 rows, 1 mm for the rest, and the measurement spacing inside a row is 1 mm. The hardness distribution is then contoured basing on the recorded measurements.

2.4. Nanoscratch test

The scratch tests are performed on a Keysight G200 set up by using a Berkovich tip. The samples are sliced from the worn zone of the outer ring. The normal loads of 100 mN, 200 mN, 300 mN and 400 mN are chosen, and the scratch length is 200 μm along the axial direction, with a scratch speed of 0.5 μm/s. Three scratch tests are carried out at near zone to conform the results repeatability, and the samples for nano-scratch are prepared by mechanically polished methods as discribed in

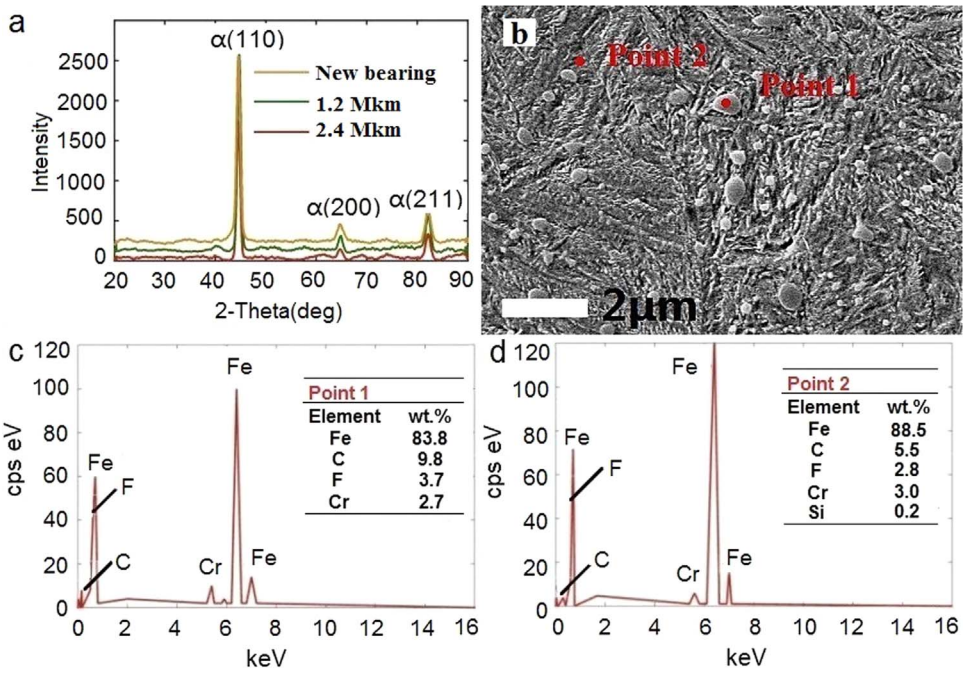

Fig. 3. Phase composition characterization: (a) XRD pattern of different mileages; (b) SEM micrograph of the bearing outer ring material (2.4 Mkm); (c) precipitation cementite element composition at point 1 in (b); (d) martensite laths element composition at point 2 in (b). The energy dispersive spectrometer (EDS) analysis shows that the particles are composed primarily of higher C element compared with the average chemical composition of other elements, as illustrated in Fig. 2c and d.

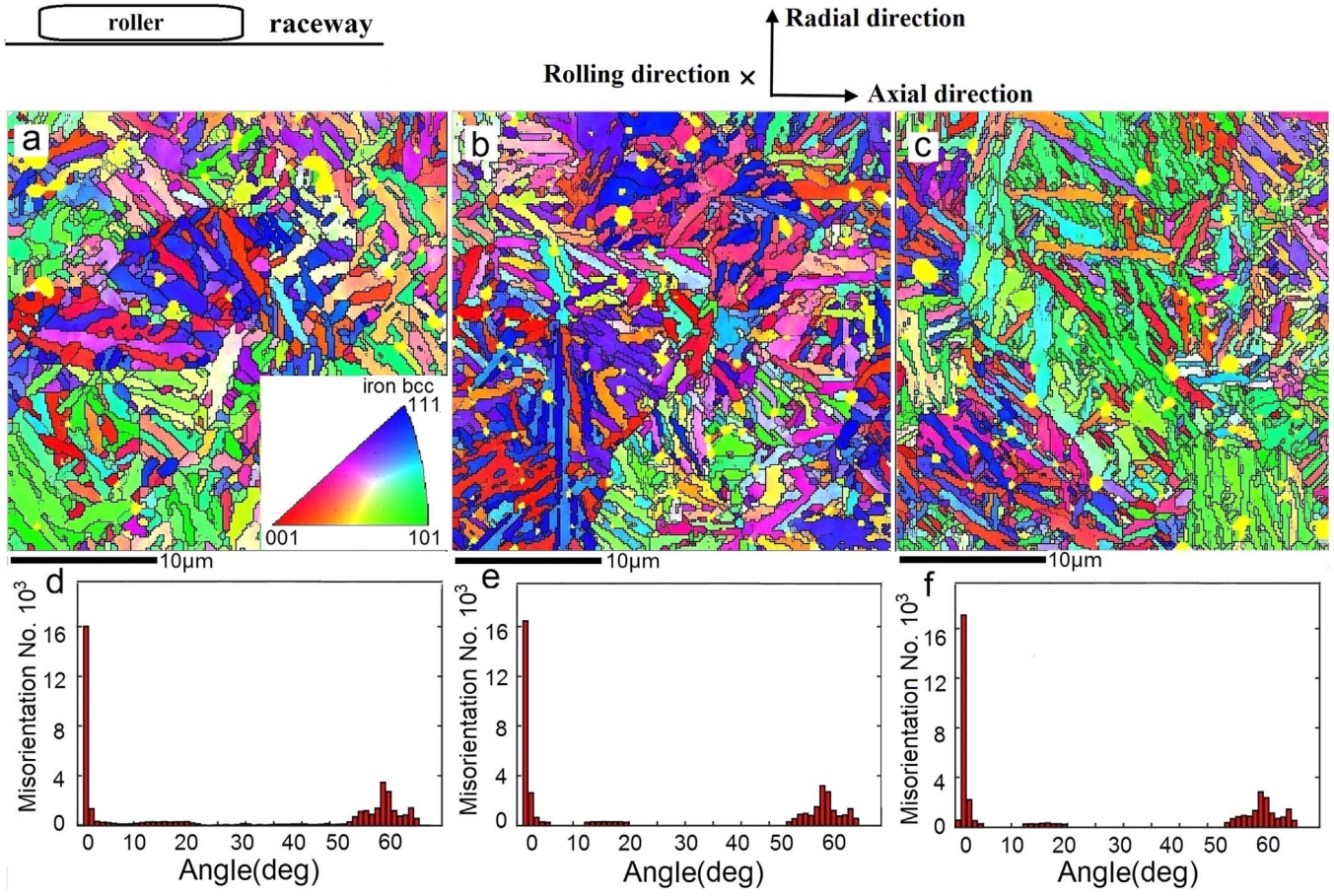

Fig. 4. Microstructure characterization from EBSD analysis: (a), (b), (c) grain type and size distributions for new, 1.2 Mkm and 2.4 Mkm bearing outer rings, respectively; (d), (e), (f) grain boundary angle statistics for new, 1.2 Mkm and 2.4 Mkm bearing outer rings, respectively.

the hardness section.

3. Results and discussions

3.1. Microstructure characterization

We investigate the microstructure evolution in the bearing outer rings at different operating durations. Fig. 3a gives the X-ray diffraction patterns for samples from bearings in brand-new, 1.2 Mkm and 2.4 Mkm operating mileage conditions. Even former literature [19] mentioned that nano-ferrites can be generated during rolling contact fatigue of bearing steel. Several groups also reported [23–27] that the transformation of retained austenite to martensite was the primary mechanism during rolling. However, in this paper, the X-ray diffraction patterns in Fig. 3a show that the phase structure of the outer ring materials is mainly b.c.c martensite, with no identifiable peaks of retained austenite, which shows no evidence of phase change after 2.4 Mkm. The SEM micrograph for the typical 2.4 Mkm sample is shown in Fig. 3b. Combined with energy dispersive spectrometer (EDS) analysis, it reveals that the outer ring material consists mainly of martensite laths (Fig. 3d) with some precipitation cementite (Fig. 3c). The cementite is believed to be responsible for the hardening characteristic of the bearing material and has a strong influence on the anti-fatigue properties of these steels [28].

Fig. 4 shows the EBSD analysis [29,30] for new, 1.2 Mkm and 2.4 Mkm bearing outer ring materials in the loading zones. We conform that the materials are primarily consisted of martensite laths from phase calibration, in agreement with the previous XRD and EDS results. The average grain sizes are 0.77 μm, 0.64 μm and 0.50 μm, respectively, meaning a 6.1% and 21.9% grain refinement after one and two operating durations (Fig. 4a, b and c). The maximum normal and shear contact stress for the present bearing is about 1177 MPa and 351 MPa, respectively [31]. Rolling is a typical way of surface loading which could harden the contact pairs [32] or fatigue them [19], depending on specific contact conditions and contact materials whether have hardening margin. Basing on the grain refinement results above, classical Hall-Patch relationship [33,34] pointed out that grain refinement may result in material strengthening in polycrystalline metals. Along with the grain refinement analysis, Fig. 4d, e and f also show the grain boundary angle statistics between adjacent grains, and it can be seen that the numbers of small-angle grain boundaries do not change nearly, indicating that the tested bearing steels have no clue of structure evolution after 2.4 Mkm from the view of the grain boundary angle distributions aspects.

Li et al. [35] noticed that the refinement of martensitic laths may harden the stainless bearing steels. Several groups [13,14,36–38] also showed that multi-level architecture structured metals from rolling or torqueing [15] grain refinement method can overcome the material strength-ductile tradeoff. So it is interesting to examine whether the bearing outer ring has been hardened or strengthened after rolling for more than 8×10^8 cycles (2.4 Mkm).

3.2. Uniaxial tensile

The ultimate tensile strength for the new, 1.2 Mkm and 2.4 Mkm bearing samples is 2.53 GPa, 2.44 GPa and 2.40 GPa, respectively (Fig. 5). It can be seen that the tensile strength of the bearing outer ring has a reduction of less than 5%, the yielding strength remains nearly the same after operation for 2.4 Mkm, and the elongation for different operating duration samples is 4.3%, 3.1% and 2.5%, respectively (Fig. 5). It is widely accepted that both phase transformation from austenite to martensite [39] and grain refinement and increment of small-angle grain boundaries [40] can improve the strength of the bearing steels; However, in this investigation, we see that the outer ring material consists mainly of martensite laths; there is neither an indication of phase transformation nor increase in small-angle grain boundaries (Figs. 3 and 4) after 2.4 Mkm operation, and the only obvious micro-structure changing we observed is the grain refinement (Section 3.1). Basing on the traditional Hall-Petch theory about the relationship between grain size and strength, the tensile strength should be increased due to the refined grains. We see in the opposite reduced strengths of bearings with different running time. This peculiar result is attributed to the fatigue damage accumulated in the bearings during their operating duration. On the other side, the fractographs for new, 1.2 Mkm and 2.4 Mkm bearing samples are examined, and it is seen that the fracture cracks were all initiated from the material inclusion zones (as shown in Fig. 6), but for the 1.2 or 2.4 Mkm samples, they have more and bigger micro-cracks near the initiated zones, and we believe that these phenomenon are also evidences for the fatigue damage accumulation for different operating duration bearings. The reduced ductility is also a resultant of aforementioned fatigue mechanism.

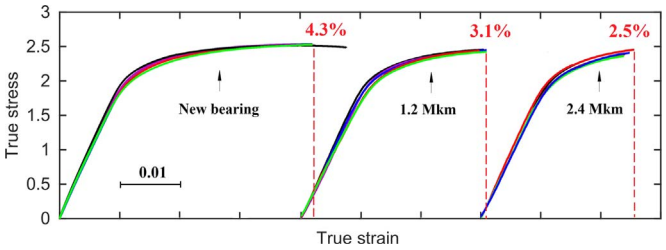

Fig. 5. Tensile stress strain curves of uniaxial samples for new, 1.2 Mkm and 2.4 Mkm bearing. A degradation of tensile ductility with operating duration is clearly seen.

3.3. Microhardness characterization

The hardness distribution across the outer rings for new, 1.2 Mkm and 2.4 Mkm bearing are shown in Fig. 7. For the new bearing, the hardness has an uniform distributions with an average value of 720 ± 10HV (Fig. 7a). For the 1.2 Mkm bearing, the hardness is no longer uniform (Fig. 7b). There are local hardened domains within the middle region. The 2.4 Mkm sample exhibits significantly hardening near the outer edge of the contact zone. The local hardened zone has a typical thickness of 2 mm (Fig. 7c). The average hardness of the 2.4 Mkm samples is about 20 HV greater than that of as-received bearings. Hardness increase can be resulted from micro-structure change such as phase transformation, grain refinement and work-hardening etc. Siva et al. [24] pointed out that the hardness of GCr15 bearing steel after heat plus deep cryogenic treatment is about 18% higher than that of the heat treated ones. Xie et al. [41] reported that the chrome molybdenum steel's hardness increased about 50% at the contact surface zone area, owning to the local plastic work-hardening effect. Arakere et al. [42] also mentioned that plastic strain accumulation around carbide inclusions in bearing steel can result in a maximum steel hardness increasing of about 12% after 13.5×10^6 operating cycles. In this paper, as we see that there are no perceivable peaks of retained austenite or new phases after 2.4 Mkm operation (Fig. 3a), so the gradient distribution of hardness or local hardened zones may have no apparent connection with phase transformation. From the grain refinement results in 3.1 section (the grain size of 2.4 Mkm operation is about 21.9% smaller than that in the new bearing), and also the plasticity reduce results in 3.2 section, we concluded that the bearing steel hardening is mainly contributed by grain refinement and work-hardening.

3.4. Scratch toughness

Scratch is a compound process involving cutting (creation of new surface) and large deformation of the test material. The scratch toughness, an intrinsic material parameter defined as the normalized energy consumption during the scratch process [43], is one of the most important parameter to characterizing the material's ability to against

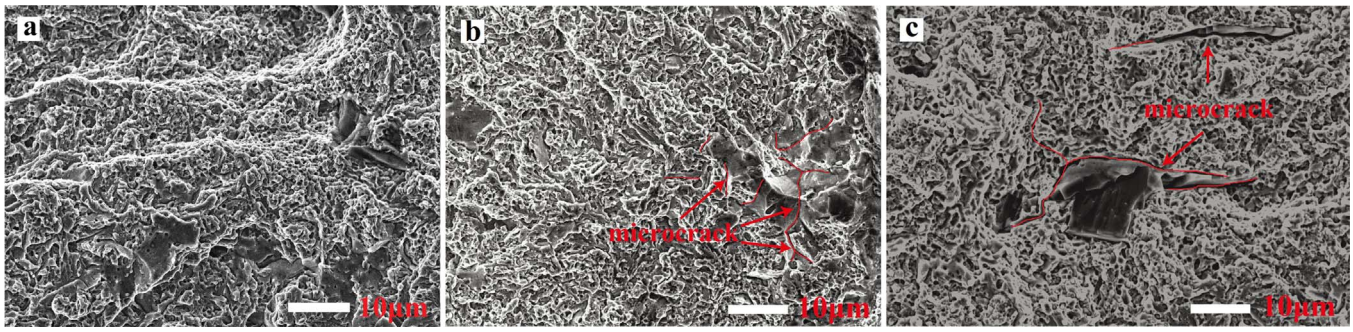

Fig. 6. SEM fractographs for new (a), 1.2 Mkm (b) and 2.4 Mkm (c) bearing uniaxial tensile samples, and it is seen that the fracture cracks were all initiated from the material inclusion zones, but for the 1.2 or 2.4Mkm samples, which have more and bigger micro-cracks near the initiated zones.

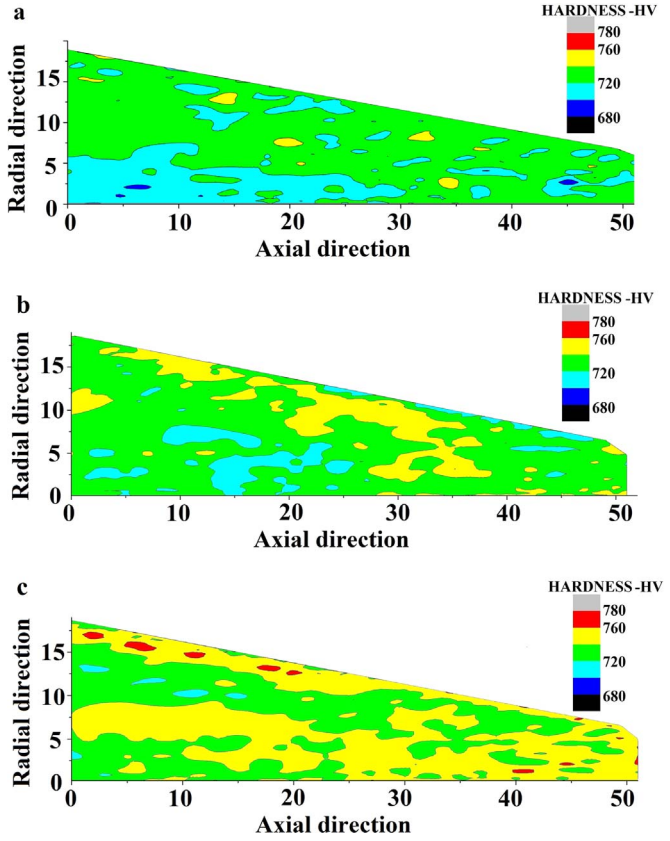

Fig. 7. Micro-hardness contour: (a) new, (b) 1.2 Mkm and (c) 2.4 Mkm bearing across the bearing outer ring cross-section.

fracture and wear. Hence, it is of interest to know the outer ring scratch toughness evolution after different bearing service durations.

Four typical lateral scratch force F_l at different normal force F_n (100 mN, 200 mN, 300 mN and 400 mN) for new, 1.2 Mkm and 2.4 Mkm bearing outer ring is shown in Fig. 8a, and it can be seen that the lateral force keeps stable approximately for each scratch, which implies a stable physical process during the scratch. The corresponding average friction coefficient is 0.10 ± 0.01, 0.17 ± 0.01, 0.30 ± 0.01 and 0.29 ± 0.01, respectively. We can conclude that the rolling progress has a slight effect on the friction coefficient. A typical SEM image of the scratches of 400 mN normal force is shown in Fig. 8b, typical scratch cross-sectional profiles for different operating duration bearings at 400 mN are both shown in Fig. 8c which includes the definition for scratch width w and depth d. The depth of the cross profile is 908 nm, 863 nm and 831 nm, respectively, and the depth decreases about 8.5%. Lu [37] mentioned that gradient structure achieves better mechanical strength, and the strength decreases with the increase of the depth of material. The surface of the raceway shows local strengthening in the worn zone from Fig. 5b and c. Therefore, the depth of the cross profile in the new bearing is a little greater than that of the used bearing.

As crack and wear resistance are important technical parameter of the bearing, the analysis of the scratch toughness is required. The scratch toughness is defined as [43] $K_S = \sqrt{0.5F_l^2+0.3F_n^2}/(w\sqrt{d})$, the numerator $\sqrt{0.5F_l^2+0.3F_n^2}$ and denominator $w\sqrt{d}$ data of the scratch tests for new, 1.2 Mkm and 2.4 Mkm bearings are plotted in Fig. 8d. The scratch toughness for the new, 1.2 Mkm and 2.4 Mkm bearings are 32.7 MPa $\sqrt{m}$, 30.3 MPa $\sqrt{m}$ and 28.7 MPa $\sqrt{m}$, respectively. So it can be seen that the fracture toughness measured from scratch tests has no significant change following operation. We note that more elaborated characterization is desired for a sound conclusion to be made.

4. Conclusions

Axle bearing plays an extremely important role in railway safety. The contact zone of outer ring is the most vulnerable region. In the paper, we examined the microstructure evolution and mechanical properties of GCr15 steel used for bearings in HSR. Major conclusions are given below:

- The phase structure of the outer ring materials shows little difference between the as-received one and that after 2.4 Mkm operation. However, grain refinement is clearly observed, from 0.77 μm in the as-received sample to about 0.50 μm in the sample after 2.4 Mkm operation.
- The ultimate tensile strength of the outer ring decreases slightly after 2.4 Mkm operation, but the elongation in the worn surface of the raceway shows a notable degradation by about 42% in bearings outer ring with that operating duration.
- Rolling of the outer ring resulted in inhomogeneous hardness distribution, with higher hardness near the edge of the outer ring, are mainly resulted from the grain refinement and plastic work-hardening. The typical dimension of the hardened zone is about 2 mm after 2.4 Mkm operation.

Acknowledgements

The authors acknowledge support from the Strategic Priority Research Program of the Chinese Academy of Sciences (XDB22020200), the National Key Research and Development Program of China (2016YFB1200403), and the Ministry of Railways Science and Technology Division of China (2013J008-C-01).

Appendix A. Supporting information

Supplementary data associated with this article can be found in the online version at http://dx.doi.org/10.1016/j.wear.2017.10.016.

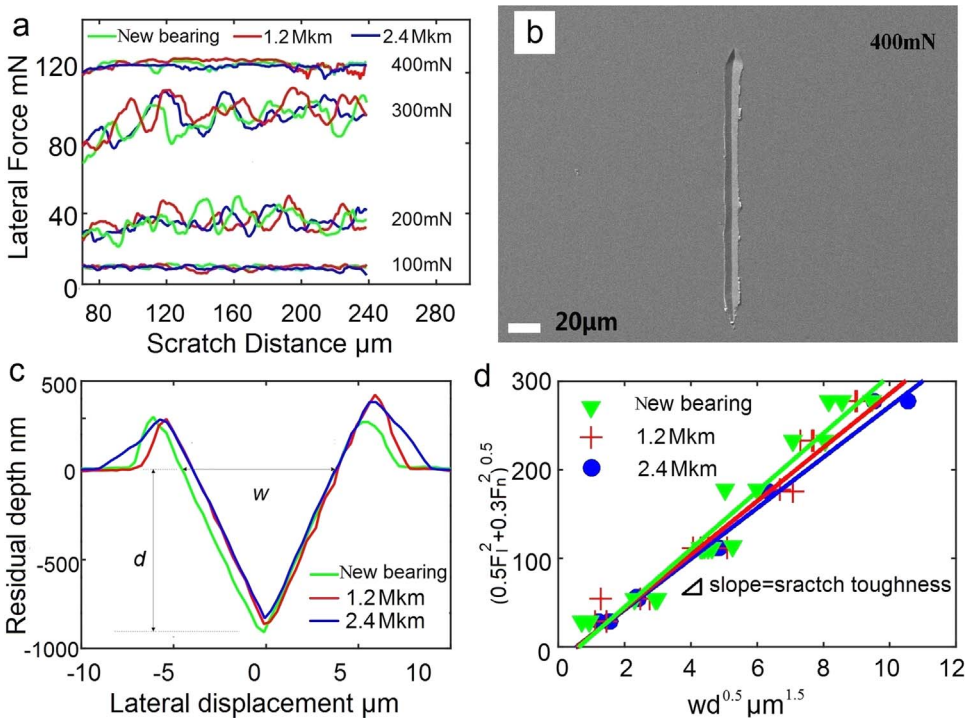

Fig. 8. The nano-scratch properties of the outer rings for new, 1.2 Mkm and 2.4 Mkm bearing: (a) lateral forces at normal force of 100 mN, 200 mN, 300 mN and 400 mN; (b) a typical SEM image for scratch at normal force of 400 mN for the 2.4 Mkm bearing; (c) three typical cross-sectional profiles of the residual scratches at normal force of 400 mN; (d) the linear fitted scratch toughness K_S = 32.7MPa$\sqrt{m}$, 30.3MPa$\sqrt{m}$ and 28.7MPa$\sqrt{m}$ for new, 1.2 Mkm and 2.4 Mkm bearings, respectively.

References

[1] H. Bhadeshia, Steels for bearings, Prog. Mater. Sci. 57 (2012) 268–435.
[2] F. Massi, N. Bouscharain, S. Milana, J.G. Le, Y. Maheo, Y. Berthier, Degradation of high loaded oscillating bearings: numerical analysis and comparison with experimental observations, Wear 317 (2014) 141–152.
[3] T.A. Harris, Rolling bearing analysis, John Wiley and Sons Inc, New York, 1991.
[4] A. Warhadpande, F. Sadeghi, M.N. Kotzalas, G. Doll, Effects of plasticity on subsurface initiated spalling in rolling contact fatigue, Int J. Fatigue 36 (2012) 80–95.
[5] N. Raje, F. Sadeghi, R.G. Rateick, A statistical damage mechanics model for subsurface initiated spalling in rolling contacts, J. Tribol. 130 (2008) 786–791.
[6] N. Raje, T. Slack, F. Sadeghi, A discrete damage mechanics model for high cycle fatigue in polycrystalline materials subject to rolling contact, Int J. Fatigue 31 (2009) 346–360.
[7] Z.Q. Lei, A.G. Zhao, J.J. Xie, C.Q. Sun, Y.S. Hong, Very high cycle fatigue for GCr15 steel with smooth and hole-defect specimens, Theor. Appl. Mech. Lett. 2 (2012) 031003.
[8] J.A. Williams, Wear and wear particles-some fundamentals, Tribol. Int. 38 (2005) 863–870.
[9] R. Nilsson, R.S. Dwyer-Joyce, U. Olofsson, Abrasive wear of rolling bearings by lubricant born particles, Proc. Inst. Mech. Eng. Part J. J. Eng. Tribology 220 (2006) 429–439.
[10] M. Scherge, D. Shakhvorostov, K. Pohlmann, Fundamental wear mechanisms of metals, Wear 255 (2007) 395–400.
[11] Y.C. Tasan, M.B. Rooij, D.J. Schipper, Changes in the microgeometry of a rolling contact, Tribol. Int. 40 (2007) 672–679.
[12] K. Lu. New Frontiers of Nanometals, in: Proceedings of the 35th Riso International Symposium on Materials Science, Department of Wind Energy, Denmark; 2014, pp. 89.
[13] K. Lu, J. Lu, Surface nanocrystallization of metallic materials-presentation of the concept behind a new approach, J. Mater. Sci. Technol. 15 (1999) 193–197.
[14] K. Lu, Making strong nanomaterials ductile with gradients, Science 345 (2014) 1454–1455.
[15] Y.J. Wei, et al., Evading the strength-ductility trade-off dilemma in steel through gradient hierarchical nanotwins, Nat. Commun. 5 (2014) 3580.
[16] Z.W. Ma, J.B. Liu, G. Wang, H.Y. Wang, Y.J. Wei, H.J. Gao, Strength gradient enhances fatigue resistance of steels, Sci. Rep. 6 (2016) 22156.
[17] Z.B. Wang, N.R. Tao, S. Li, W. Wang, G. Liu, J. Lu, K. Lu, Effect of surface nanocrystallization on friction and wear properties in low carbon steel, Mater. Sci. Eng. A 352 (2003) 144–149.
[18] J.H. Kang, R.H. Vegte, P.E.J. Rivera-Díaz-del-Castillo, Rolling contact fatigue in martensitic 100Cr6: subsurface hardening and crack formation, Mater. Sci. Eng. A 607 (2014) 328–333.
[19] S.X. Li, Y.S. Su, X.D. Shu, J.J. Chen, Microstructural evolution in bearing steel under rolling contact fatigue, Wear 380–381 (2017) 146–153.
[20] J. Burbank, M. Woydt, Optimization of pre-conditioned cold work hardening of steel alloys for friction and wear reductions under slip-rolling contact, Wear 350-351 (2016) 141–154.
[21] B. Mahmoudia, G.L. Dolla, C.H. Hager Jr, R.D. Evans, Influence of a WC/a-C: H tribological coating on micropitting wear of bearing steel, Wear 350- 351 (2016) 107–115.
[22] H.K. Danielsen, F. Gutiérrez Guzmán, K.V. Dahl, Y.J. Li, J. Wu, G. Jacobs, G. Burghardt, S. Fæster, H. Alimadadi, S. Goto, D. Raabe, R. Petrov, Multiscale characterization of White Etching Cracks (WEC) in a 100Cr6 bearing from a thrust bearing test rig, Wear 370–371 (2017) 73–82.
[23] A.P. Voskamp, E.J. Mittemeijer, Crystallographic preferred orientation induced by cyclic rolling contact loading, Metall. Mater. Trans. 27 (1996) 3445–3465.
[24] R. Sri Siva, M. Arocki Jaswin, D. Mohan Lal, Enhancing the wear resistance of 100Cr6 bearing steel using cryogenic treatment, Tribology Trans. 55 (2012) 387–393.
[25] M. Arockia Jaswin, D. Mohan Lal, Optimization of the Cryogenic Treatment Process for En 52 Valve Steel Using the Grey-Taguchi Method, Mater. Manuf. Process. 25 (2010) 842–850.
[26] Iris V. Riveroa, Clayton, O. Ruud, Deviation of residual stress patterns in 52 100 bearing steel due to inherent microstructural transformations after rolling contact, Mater. Charact. 53 (2004) 381–393.
[27] V. Rivero Iris, O. Ruud Clayton, Residual stresses and patterns in 52 100 bearing steel: preliminary analysis of strain hardening vs. microstructural transformation by XRD analysis, Lubr. Eng. 58 (2002) 30–40.
[28] A.S. Pandkar, N. Arakere, G. Subhash, Microstructure-sensitive accumulation of plastic strain due to ratcheting in bearing steels subject to Rolling Contact Fatigue, Int. J. Fatigue 63 (2014) 191–202.
[29] H. Matsunaga, H. Komata, J. Yamabe, Y. Fukushima, S. Matsuoka, Effect of size and depth of small defect on the rolling contact fatigue strength of bearing steel JIS-SUJ2, Procedia Mater. Sci. 3 (2014) 1663–1668.
[30] H. Fu, E.I. Galindo-Nava, P.E.J. Rivera-Díaz-del-Castillo, Modelling and characterization of stress-induced carbide precipitation in bearing steels under rolling contact fatigue, Acta Mater. 128 (2017) 176–187.
[31] Y.J. Hao, Reliability modeling and research of the axle box roller bearing used in High-speed train, Beijing Jiaotong University, Beijing, 2014 (In Chinese).
[32] M. Miller, C. Bobko, M. Vandamme, F.J. Ulm, Surface roughness criteria for cement paste nanoindentation, Cem. Concr. Res. 38 (2008) 467–476.
[33] E.O. Hall. The deformation and ageing of mild steel, in: Proceedings of the Physical Society of London, UK, 1951, pp. 495–502.
[34] N.J. Petch, The cleavage strength of polycrystals, J. Iron Steel Inst. 174 (1953) 25–28.
[35] S.H. Li, X.H. Yuan, W. Jiang, H.D. Sun, J. Li, K.Y. Zhao, M.S. Yang, Effects of heat treatment influencing factors on microstructure and mechanical properties of a low-carbon martensitic stainless bearing steel, Mater. Sci. Eng. A 605 (2014) 229–235.
[36] T.H. Fang, W.L. Li, N.R. Tao, K. Lu, Revealing extraordinary intrinsic tensile plasticity in gradient nano-grained copper, Science 331 (2011) 1587.
[37] H.T. Wang, N.R. Tao, K. Lu, Architectured surface layer with a gradient nanotwinned structure in a Fe–Mn austenitic steel, Scr. Mater. 68 (2013) 22–27.
[38] G.W. Yang, X.J. Sun, Z.D. Li, X.X. Li, Q.L. Yong, Effects of vanadium on the microstructure and mechanical properties of a high strength low alloy martensite steel, Mater. Des. 50 (2013) 102–107.
[39] A.G. Kalashami, A. Kermanpur, A. Najafizadeh, Y. Mazaheri, Development of a high strength and ductile Nb-bearing dual phasesteel by cold-rolling and intercritical annealing of the ferrite-martensite microstructures, Mater. Sci. Eng. A 658 (2016)

355–366.
[40] A.M. Guo, R.D.K. Misra, J.B. Liu, L. Chen, X.L. He, S.J. Jansto, An analysis of the microstructure of the heat-affected zone of an ultra-low carbon and niobium-bearing acicular ferrite steel using EBSD and its relationship to mechanical properties, Mater. Sci. Eng. A 527 (2010) 6440–6448.
[41] L.C. Xie, Q.H. Zhou, W. Yan, L.Q. Wang, W.J. Lu, Microstructure variation and local plastic response of chrome molybdenum alloy steel after quasi rolling contact fatigue testing, Mater. Sci. Eng. A 659 (2016) 37–46.
[42] N.K. Arakere, G. Subhash, Work hardening response of M50-NiL case hardened bearing steel during shakedown in rolling contact fatigue, Mater. Sci. Technol. 28 (2012) 34–38.
[43] A.T. Akono, F.J. Ulm, Scratch test model for the determination of fracture toughness, Eng. Fract. Mech. 78 (2011) 334–342.